pH Effect on the H 2 O 2 -Induced Deactivation of Fe-N-C Catalysts

Geunsu Bae, Min Wook Chung, Sang Gu Ji, Frédéric Jaouen, Chang Hyuck Choi

pH effect on the H_2O_2-induced deactivation of Fe-N-C catalysts

Geunsu Bae,[†,§] Min Wook Chung,[†,§] Sang Gu Ji,[†] Frédéric Jaouen,[‡] and Chang Hyuck Choi*[†]*

[†]School of Materials Science and Engineering, Gwangju Institute of Science and Technology, 61005 Gwangju, Republic of Korea.

[‡]ICGM, Univ. Montpellier, CNRS, ENSCM, Montpellier, France.

ABSTRACT Despite a promising activity of Fe-N-C catalysts at beginning-of-life in proton-exchange membrane fuel cells (PEMFCs), their poor durability in operating PEMFCs remains a great challenge for the successful replacement of commercial Pt-based catalysts. One of the key reasons for this poor *operando* durability is the surface oxidation of carbonaceous supports *via* Fenton(-like) reactions between the Fe centers and the intermediate product of the oxygen reduction reaction (ORR) in acidic medium, H_2O_2. In the present study, we have investigated the pH effect on the chemical deactivation of Fe-N-C catalysts by contacting with controlled amount of H_2O_2. Covering the entire pH range 0–14, we reveal a strong pH dependence of the H_2O_2-induced deactivation. Especially, acidic H_2O_2 treatment leads to a severe decrease in ORR activity while almost negligible deactivation is found after the treatment in sufficiently strong alkaline electrolyte. Electron paramagnetic resonance (EPR) study reveals a positive correlation between the magnitude of Fe-N-C activity decrease and the signal intensity of hydroxyl radical spin adduct after H_2O_2 treatment at a given pH. Reactive oxygen species (ROS) such as the hydroxyl radical is identified as a key deactivating agent of Fe-N-C catalysts operating from acidic to neutral pH environments. This result suggests that controlling the formation and lifetime of ROS at such pH is crucial to secure durable fuel cell operation with Fe-N-C cathodes. Alternatively, fuel cell operation under highly alkaline environment could also be considered to improve the catalytic durability, by virtue of different Fenton(-like) reaction pathway at such pH.

KEYWORDS: Fe-N-C catalysts, durability, degradation, hydrogen peroxide, Fenton reaction

INTRODUCTION

Fe-N-C catalysts comprising atomically dispersed Fe cations ligated with N-functionalities on carbon supports (FeN$_x$C$_y$ active moieties) are the most promising materials to replace the rare platinum in PEMFC cathodes.[1-7] Tremendous efforts have been devoted to improve the beginning-of-life activity and power performance of Fe-N-C catalysts and cathodes, consequently accomplishing a promising initial performance (~1 W cm^{-2}) in PEMFCs.[1, 8-9] Despite significant recent improvements in their initial activity, the successful market introduction of Fe-N-C catalysts now faces a serious challenge, namely their poor durability in operating conditions.[10-11] In acidic PEMFC conditions, Fe-N-C catalysts have shown severe activity decay within tens of hours of operation at a voltage range of 0.4–0.6 V$_{RHE}$.[12-14] Fe-demetalation, protonation of N-functional groups, carbon corrosion, and H$_2$O$_2$-induced surface oxidation have been suggested as possible degradation routes for Fe-N-C catalysts.[10, 15-18] In particular, subtle modifications of the carbon surface chemistry induced by reaction of Fe-N-C with the H$_2$O$_2$ (byproduct of the ORR) have been recently pointed out as one of the major deactivation mechanisms of Fe-N-C catalysts in acidic environments.[18-22]

The *in operando* formed H$_2$O$_2$ molecules can chemically react with Fe species (including FeN$_x$C$_y$ active moieties) through the well-known Fenton(-like) reactions, producing ROS such as the hydroxyl, hydroperoxyl, and superoxide radicals. In turn, the ROS can oxidize the carbon top-surface, populating it with oxygen functional groups, both at long distance from FeN$_x$ centers but also on carbon sites adjacent to the FeN$_x$ centers. Goellner *et al.* reported decreased ORR activity of Fe-N-C catalysts after *ex situ* H$_2$O$_2$ treatments (a useful method to investigate the effect of ROS on catalytic activity precisely, decoupled from more complex intertwined effects that might occur *in operando* such as potential-driven demetalation or carbon corrosion), correlated with formation of oxygen functional groups on the carbonaceous

surface.[18] This modification could obviously render the surface more hydrophilic and consequently further increase the risk of flooding in the micropores hosting the active FeN_xC_y moieties. Less intuitive, it was also demonstrated that the long-range oxidation of the carbon surface decreases the intrinsic turnover frequency (TOF) of the FeN_xC_y sites *via* weakened oxygen binding on the Fe center.[21] In the latter work, the chemically-induced deactivation of Fe-N-C by H_2O_2 was studied at two different pH conditions, *i.e.*, in strongly acidic and alkaline conditions (pH values of 1 and 13). A decrease in the ORR activity of Fe-N-C was observed after the H_2O_2 treatment in acidic environment, but not in alkaline environment. Note that the actual pH at which the ORR activity was measured before/after the treatment did not change the trends, *e.g.*, similar trends in activity decrease was observed in pH 1 and 13 electrolytes after H_2O_2 treatment at pH 1. This indicates that the same sites are ORR-active in high and low pH conditions, in the Fe-N-C catalyst that was studied (comprising only FeN_xC_y moieties). These control experiments suggested a strong pH dependence of the H_2O_2-induced deactivation process and provided further insights into how the durability issue of Fe-N-C in operating fuel cells might be resolved. However, the pH dependence of the deactivation of Fe-N-C has not yet been thoroughly investigated, with only extreme pH conditions investigated (1 and 13) and without detailed explanation as to why no deactivation occurred in high pH conditions. It is therefore unclear if high pH conditions result in the absence of ROS when Fe-N-C is contacted by H_2O_2, or if ROS still form but the carbon oxidation is slowed down in alkaline pH conditions.[23] Therefore, in this study we investigated the H_2O_2-induced deactivation of a model Fe-N-C catalyst (comprising only FeN_xC_y moieties) as a function of the pH at which the catalyst was treated with H_2O_2. We covered the pH range from 0 to 14, in order to determine the origin of the pH-dependent deactivation. From the results and analyses, we eventually suggested synthetic or system-level strategies for minimizing catalytic degradation of Fe-N-C catalysts during fuel cell operation.

4

RESULTS and DISCUSSION
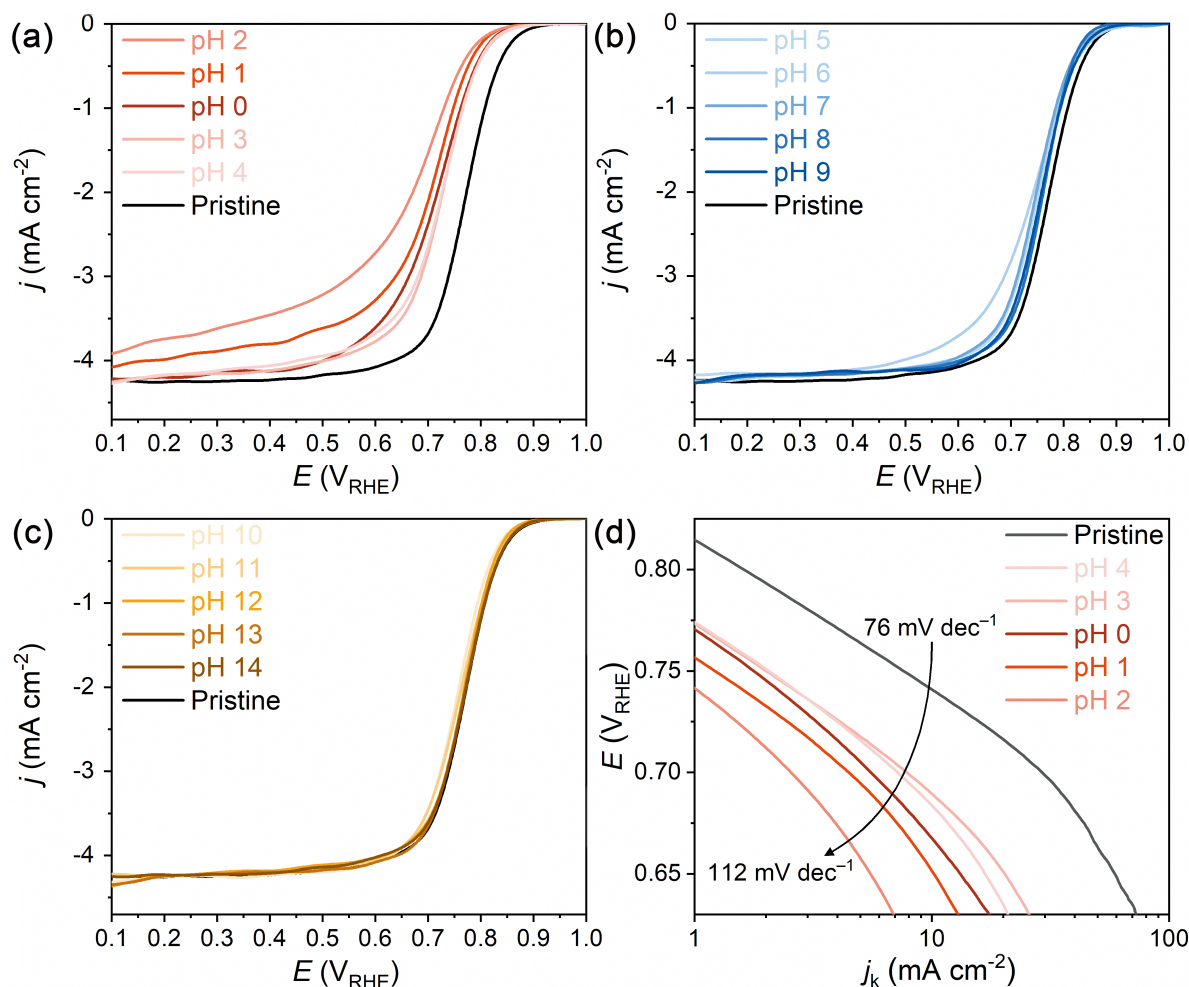
Figure 1. ORR polarization curves of the H_2O_2-treated FeNC-dry-0.5 catalytic layers. The polarization curves were measured in a 0.1 M $HClO_4$ electrolyte after the H_2O_2 treatment in (a) acidic (pH = 0–4), (b) neutral (pH = 5–9), and (c) alkaline (pH = 10–14) conditions. $HClO_4$, H_3PO_4 buffer, $KHCO_3$ buffer, and KOH solutions were used to adjust the pH in the 0–2, 3–8, 9–12, and 13–14 ranges, respectively. Ten measurements were recorded for each pH of H_2O_2 treatment, but this figure shows the most representative polarization curves. (d) Tafel plots for the FeNC-dry-0.5 catalytic layers measured after the H_2O_2 treatment in acidic conditions.

Following our previous studies,[21, 24] the Fe-N-C catalyst was synthesized by pyrolysis of a precursor mixture, which contained Fe^{II} acetate, 1,10-phenanthroline, and a Zn^{II} zeolitic imidazolate framework (ZIF-8). This catalyst was labelled FeNC-dry-0.5, with the label referring to the dry homogenization of the precursor powders and to the Fe content before pyrolysis (see the Experimental section for details). After the pyrolysis, the Fe content in the catalyst was expected to be *ca.* 1.5 wt.%, as confirmed by inductively coupled plasma mass

spectrometry (ICP-MS). As discussed in detail in our previous reports,[21,25] the catalyst is solely composed of atomically dispersed FeN_xC_y moieties, which are the main active sites in Fe-N-C catalysts for ORR, without appreciable amounts of bulk Fe species (Figure S1). Due to its unique structural characteristics, FeNC-dry-0.5 could be applied as a representative model of Fe-N-C catalysts, suitable for fundamental studies without interference from the less active (or inactive) bulk Fe species.

To investigate the pH effect on the H_2O_2-induced deactivation, FeNC-dry-0.5 was first deposited on a rotating disk electrode (RDE). The deposited catalyst was then treated for 2 h at 50 °C, with a pH-adjusted solution containing 1 wt.% H_2O_2. The solution pH was varied from 0 to 14, each pH value defining one H_2O_2-treated Fe-N-C layer. In such conditions, the H_2O_2 treatment of the catalytic layer could be continuously progressed, with significant amount of H_2O_2 remaining even after 2 h, at all pH values (Figure S2). Moreover, the decrease in H_2O_2 concentration with time is only little affected by the presence of the Fe-N-C electrode in solution. The effect of H_2O_2 treatment on the ORR activity was investigated by measuring ORR polarization curves in RDE setup of all the H_2O_2-treated Fe-N-C layers, in identical electrolyte conditions (Figure 1). To measure the ORR activity, we chose a 0.1 M $HClO_4$ (pH 1) electrolyte due to a larger magnitude of ORR activity decay seen after H_2O_2 treatment in acidic conditions compared to alkaline conditions.[26] In the latter case, the ORR activity from the N-C support is not fully negligible, dampening the activity decay after H_2O_2 treatment. The ORR polarization curves identify a strong decay of ORR activity after the H_2O_2 treatment in acidic conditions (pH range 0–4, Figure 1a), a moderate decay after treatment in near-neutral pH conditions (pH range 5–9, Figure 1b), and almost no decay after treatment in alkaline conditions (pH range 10–14, Figure 1c). Interestingly, the most severe deactivation was observed after H_2O_2 treatment at pH 2, while further decreasing the pH to 1 or 0 during the H_2O_2 treatment resulted in lower

6

deactivation (Figure 1a). Also, after treatment in the acidic conditions, changes in the diffusion-limited current density and in the Tafel slope can be seen (Figures 1a and d). The lower apparent diffusion-limited current density was explained by reduced selectivity towards the four-electron ORR (increasing H_2O_2 production),[21] and further supported by increased ring current in a rotating ring disk electrode (RRDE) measurements (Figure S3). Regarding the change in Tafel slope, it was ascribed in our previous work to a change in the rate determining step of the ORR, supported by density functional theory (DFT) calculations of ORR on FeN_x sites integrated on a strongly oxygenated N-C surface.[21]

In order to report in a concise way trends in the ORR activity seen in the polarization curves (Figure 1), we used the half-wave potential ($E_{1/2}$). Since the catalyst loading is identical for all Fe-N-C catalytic layers in this study, the use of $E_{1/2}$ as an activity descriptor is valid. It is noted however that, all other experimental parameters being fixed (rotation speed, scan rate, etc.), the $E_{1/2}$ value theoretically depends on both the exchange current density (j_0) and the Tafel slope.[27] Here, the change in $E_{1/2}$ value measured in 0.1 M $HClO_4$ electrolyte before and after the H_2O_2 treatment at a given pH is reported: $\Delta E_{1/2}$ (pH) = $E_{1/2}$ (after H_2O_2 treatment at given pH) − $E_{1/2}$ (pristine Fe-N-C layer).
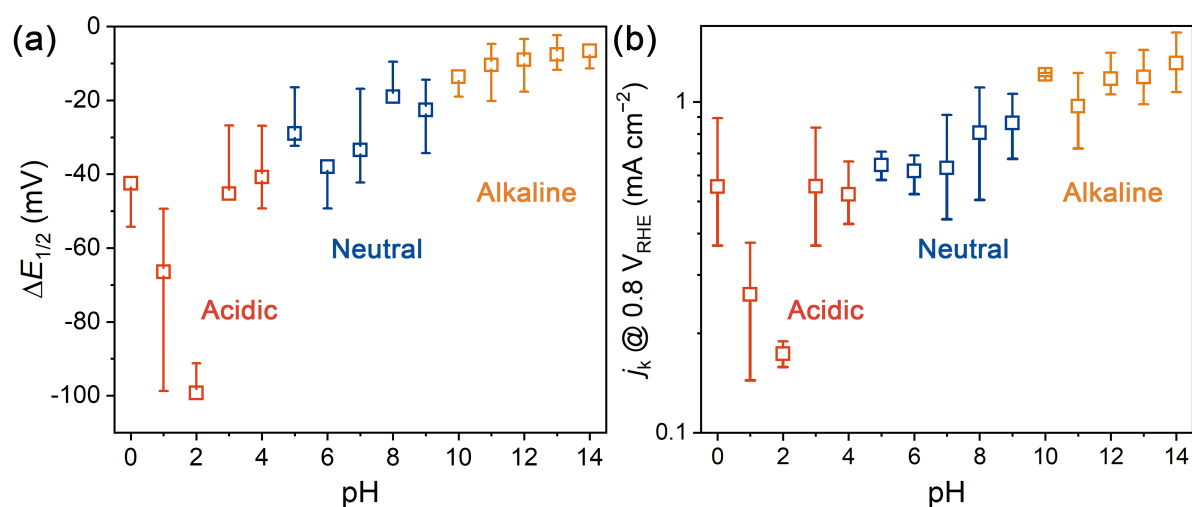
Figure 2. Correlation between the ORR activity decay for H_2O_2-treated FeNC-dry-0.5 and the pH condition used during the treatment. The H_2O_2 treatment was carried out at various pH conditions (x-axis scale), while the ORR activity was always measured in a 0.1 M $HClO_4$ electrolyte. The activity change at any given pH was analyzed in terms of (a) the difference in $E_{1/2}$ before and after the H_2O_2 treatment and (b) the j_k measured at 0.8 V_{RHE}. The error bar and average is the result of ten measurements.

The plot of $\Delta E_{1/2}$ as a function of the solution pH used during the H_2O_2 treatment is shown in Figure 2a, summarizing the trends seen in Figure 1. Acidic H_2O_2 treatments resulted in significant ORR activity drops, with $E_{1/2}$ decreasing by at least 40 mV at any pH ≤ 4 during the H_2O_2 treatment, corresponding to an activity loss of *ca*. 74 to 89% at 0.8 V_{RHE}. The most severe loss in ORR activity was measured after treatment at pH 2, with a corresponding $E_{1/2}$ decrease by *ca*. 100 mV. The large error bar seen for the deactivation extent after H_2O_2 treatment at pH 1 may be intrinsic to a change in the stability and/or type of ROS formed at pH < 1 and at pH > 1, leading to higher variability of the H_2O_2 treatment at pH 1 compared to other pH values. However, the activity decrease was progressively reduced when the pH used during the H_2O_2 treatment was increased to neutral and then alkaline conditions (Figure 2a). The $\Delta E_{1/2}$ values at near-neutral conditions (*i.e*., pH 5–9) ranged from –19 to –38 mV (an activity loss of *ca*. 36 to 52% at 0.8 V_{RHE}). After H_2O_2 treatment at pH > 9, the Fe-N-C catalyst exhibited even lower activity decrease, with $\Delta E_{1/2}$ values ranged from –7 to –14 mV (an activity loss of *ca*. 1 to 36% at 0.8 V_{RHE}). In order to represent more definite correlation between activity loss and solution pH used during the H_2O_2 treatment, we also plotted the ORR activity changes using the kinetic current density (j_k) measured at 0.8 V_{RHE} (Figure 2b), resulting similar trends with that derived from $\Delta E_{1/2}$.

Overall, these results reveal that the deactivation of FeNC-dry-0.5 is strongly pH-dependent, displaying a reverse volcano-like curve, with the highest activity drop observed after H_2O_2 treatment at *ca*. pH 2. This result is in excellent agreement with the existing knowledge of Fenton(-like) reactions' efficiency as a function of pH, when Fe is in the form of

8

solvated metal cations in solution.[28-29] This strongly suggests that the mechanism, kinetics, and type of ROS formed during Fenton(-like) reactions follow the same trends as a function of pH for Fe cations solvated in solution and for FeN_x sites covalently attached to a N-doped carbon matrix. Although the corresponding pH of the PEM environment (*e.g.*, Nafion) is close to zero,[30] the high-current operation of PEMFCs can increase the local pH at the catalyst surface to moderately acidic values,[31-32] which, according to Figure 2, is the worst pH condition for Fe-N-C catalysts when they are contacted by H_2O_2.

FeNC-dry-0.5 catalysts treated with H_2O_2 solutions of pH 1, 7, or 13 were then selected to investigate possible physicochemical changes induced by H_2O_2 treatment. X-ray diffraction (XRD), Raman spectroscopy, and Brunauer-Emmett-Teller (BET) analyses confirmed that no significant changes in the carbon structure and porosimetry occurred after the H_2O_2 treatment, regardless of the solution pH (Figure S4). This might at first sight appear in contradiction with the decreased electrocatalytic performance seen after H_2O_2 treatments at pH 1 (Figure 2). Therefore, other possible changes, such as surface composition and Fe content, were further studied by X-ray photoelectron spectroscopy (XPS) and ICP-MS, respectively. The XPS-N_{1s} signals and Fe contents (*ca.* 1.5 wt.%) were almost unchanged after the H_2O_2 treatments (Figures 3a and S5), indicating unaltered N functionalities and Fe amount. As reported previously by our group, and after using similar H_2O_2 treatment protocols,[21] the lack of changes in the first-coordination sphere of FeN_xC_y moieties before and after H_2O_2 treatment at pH 1 was demonstrated by extended X-ray absorption fine structure (EXAFS) and [57]Fe Mössbauer spectroscopy results.

The only apparent change in the sample composition concerns the oxygen content, with higher oxygen content and magnified XPS-O_{1s} signal measured after H_2O_2 treatment, compared to the pristine catalyst (Figure 3). The pristine catalyst showed an oxygen content of *ca.* 5 at.%,

while the H_2O_2-treated samples revealed oxygen content in the range of 6–9 at.% (Figure 3a). There is furthermore a clear trend of increasing oxygen content with decreasing pH of the H_2O_2 treatment solution from 13 to 7 and further to 1 (Figure 3a). This indicated that the H_2O_2 treatment introduced new oxygen functionalities on the Fe-N-C catalyst, and this surface oxidation was more significant under acidic than neutral or alkaline conditions. The XPS-O_{1s} spectrum exhibited a broad peak at *ca.* 532 eV, which could be assigned to C-O (epoxy, hydroxyl) and C=O (carbonyl, carboxyl) components, as indicated in Figure 3b. Similar trends of nitrogen and oxygen contents as identified by XPS were also measured by elemental analysis (Table S1). The oxygen content was *ca.* 3.6 at.% in the pristine catalyst, and showed increasing trend with decreasing pH of the H_2O_2 solution used to treat the catalyst. The oxygen content increased from 6.2 at.% after H_2O_2 treatment at pH 13 to *ca.* 15.3 at.% after the treatment at pH 1. In contrast, the nitrogen content stayed almost constant at *ca.* 4.9 at.%, regardless of the H_2O_2 treatment condition. Interestingly, considerable activity recovery, enabled by unmodified core-structure of the catalytic sites (FeN_xC_y), was shown after the removal of oxygen groups formed during similar H_2O_2 treatment protocols,[21] verifying that the newly generated oxygen groups deteriorate the TOF of FeN_xC_y sites.
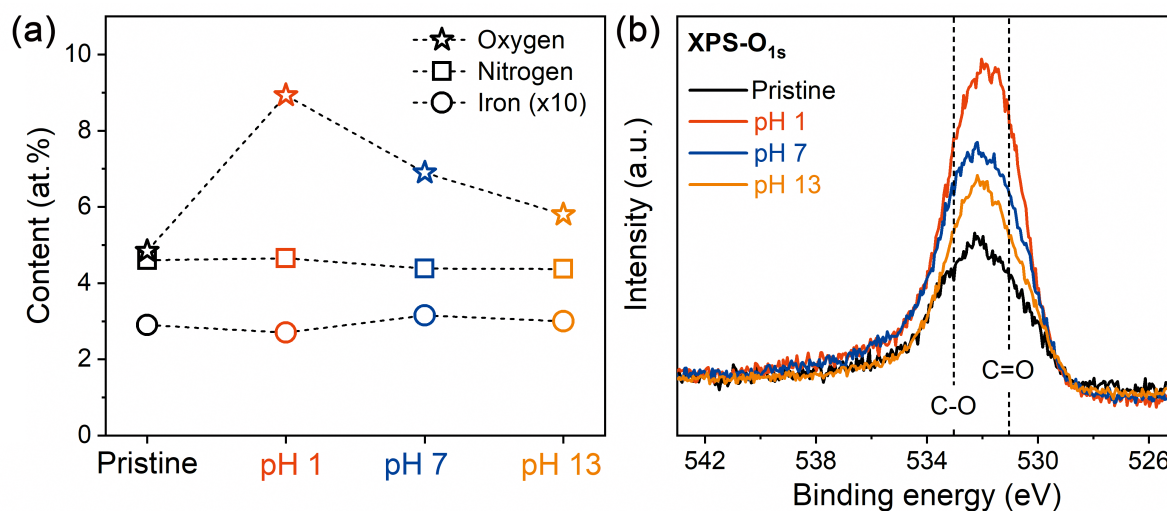
Figure 3. (a) Composition of FeNC-dry-0.5 before and after H_2O_2 treatment in different solutions. (b) XPS-O_{1s} spectra of pristine and H_2O_2-treated FeNC-dry-0.5 samples. The H_2O_2 treatment was performed at a solution pH of 1, 7, or 13.

Based on DFT calculations, our previous study predicted that the introduction of electron-withdrawing groups (*e.g.,* hydroxyl, epoxy) on the carbon surface of Fe-N-C catalysts induces an increase in the work function (WF) of the carbon support, a downshift of the Fe *d*-orbitals, and a consequent decrease in Fe oxophilicity.[21] The ORR kinetics on surface-oxidized Fe-N-C catalysts thus becomes less favourable due to decreased oxygen binding. More recently, similar conclusion was also made with a CoN_4 moiety,[33] predicting a depletion of electron density at the Co site and consequent a poor ORR kinetics as the oxygen groups are introduced. Following these computational predictions, the potential of zero charge (E_{PZC}), which has a linear relationship with the WF,[34] was thus measured for the pristine and H_2O_2-treated catalysts (Figure 4a). As the pH condition of the H_2O_2 treatment became more acidic, the E_{PZC} value increased, leading to a negative correlation between $\Delta E_{1/2}$ and E_{PZC} (Figure 4b). Meanwhile, due to known acidic properties of the oxygen functional groups identified by XPS, marked changes in surface acido-basicity (ΔpH_f) were also observed after acidic H_2O_2 treatment (Figure 4c). The negative values of ΔpH_f for all H_2O_2-treated samples indicate a more acidic character of the surface compared to the pristine catalyst. A positive correlation between $\Delta E_{1/2}$ and ΔpH_f is identified (Figure 4d), revealing that increased surface acidity (decreased ΔpH_f) results in decreased ORR activity. These two linear correlations (Figures 4b and d) indicate a negative correlation between the extent of surface oxidation of FeNC-dry-0.5 occurring during the H_2O_2 treatment and its ORR activity measured in pH 1 solution after the H_2O_2 treatment. Moreover, the correlations show that the extent of surface oxygen is modulated by the pH at which the H_2O_2 treatment is performed.

11

The observed pH dependence of the H_2O_2-induced deactivation is in qualitative agreement with numerous previous studies on the Fenton oxidation process, employed to degrade organic compounds with H_2O_2 and Fe cations solvated in solution. It was shown that the Fenton process is highly efficient in acidic environments (pH 2–3 in particular), but becomes gradually less efficient with increasing pH.[28,29,35,36] This trend has often been explained by the occurrence of different Fe phases depending on the pH conditions. For instance, the stable form of Fe salts (*e.g.*, Fe sulfate and chloride) in acidic conditions is ferric or ferrous ion, while in neutral or alkaline conditions the Fe cations precipitate as Fe hydroxide/oxides.[37] Considering the higher metal dispersion (or sometimes the better TOF) of homogeneous catalysts than those of heterogeneous catalysts,[38] this explanation based on the Fe phases appears plausible. On the other hand, the pH-dependent Fenton reactivity has also been interpreted in terms of mechanistic changes in the Fenton(-like) reactions. For example, the preferential formation of hydroxyl radical in acidic conditions but of ferryl radical in alkaline conditions has been proposed, with different reactivity of the radicals.[39] Alternatively, different kinetics of ROS generation with pH conditions has been also proposed.[40-42] Since the Fe species in FeNC-dry-0.5 is ionic Fe ligated onto N-doped carbon support, highly stable in acidic media (as long as ORR does not take place)[12,43] and also highly stable in alkaline media[44] even during ORR, one can assume that the nature of the sites immersed in the different pH electrolytes is retained in the present deactivation conditions. Based on similar Fe content before and after H_2O_2 treatment (Figure 3a), we can also rule out the Fe dissolution and precipitation degradation mechanism for the pH-dependent catalytic deactivation observed in the present conditions, *i.e.*, no ORR taking place and Fe-N-C only contacted by H_2O_2 under OCP conditions. Hence, it can be surmised that the pH dependence of the H_2O_2 treatment seen in our case is more likely due to a mechanistic change of the Fenton process as a function of the pH, rather than due to a change of Fe speciation as function of pH.
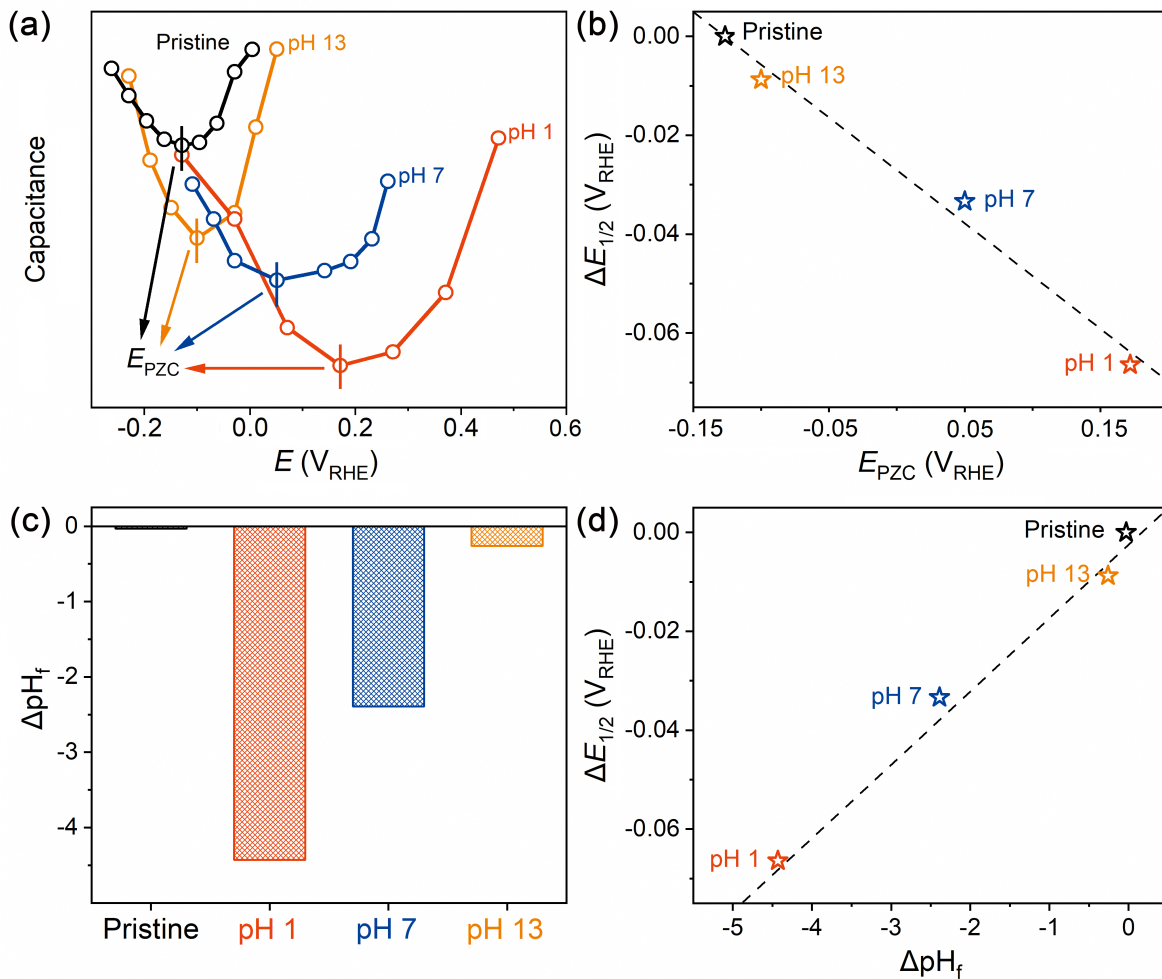
Figure 4. Changes in surface properties of FeNC-dry-0.5 induced by H_2O_2 treatment and correlations between surface properties and ORR activity measured after the H_2O_2 treatment. (a) Curves of electrochemical capacitance *vs*. electrochemical potential, used to determine E_{PZC} as a function of the pH of the H_2O_2 solution (pH 1, 7, or 13). (b) Correlation between $\Delta E_{1/2}$ measured in 0.1 M $HClO_4$ electrolyte and E_{PZC}. (c) ΔpH_f after H_2O_2 treatment at pH 1, 7, or 13. (d) Correlation between $\Delta E_{1/2}$ measured in 0.1 M $HClO_4$ electrolyte and ΔpH_f. The correlations between j_k and E_{PZC} or ΔpH_f can also be found in Figure S6.

To identify whether the pH condition applied during the H_2O_2 treatment of FeNC-dry-0.5 influences the nature of the formed ROS, EPR analyses were conducted with a nitrone spin trap (5,5-dimethyl-1-pyrroline N-oxide, DMPO). The EPR spectra were measured immediately after filtering solutions of FeNC-dry-0.5 immersed in H_2O_2-containing solution of a given pH. The EPR spectrum showed an intense quartet signal with a 1:2:2:1 intensity ratio only at pH 2 (Figure 5a), the pH at which the most severe ORR deactivation occurred. The quartet signal was unambiguously assigned to the •DMPO-OH spin adduct, identifying the ROS formation

(hydroxyl radical in particular) during the H_2O_2 treatment at pH 2. Although the quartet of the •DMPO-OH adduct was the only EPR signal observed at pH 2, the formation of other ROS cannot be ruled out because other •DMPO-ROS adducts have a shorter lifetime than •DMPO-OH and quickly break down to •DMPO-OH adduct.[45]

In contrast, the •DMPO-OH signal was very weak and hardly distinguishable from the background noise at any other pH conditions (Figure 5a). We wondered if it might be related to the preferential location of FeN_x sites in micropores (pore size < 2 nm). This location could imply that most ROS formed on FeN_x sites react with the carbon surface inside the micropores, before they diffuse out of the micropores and may be trapped by DMPO. In the opposite direction, the large molecular size of DMPO or its interaction with the Fe-N-C surface might have prevented its efficient diffusion into micropores. In the search for a material with similar FeN_x sites than in FeNC-dry-0.5 but with increased accessibility of Fe by DMPO, we selected Fe^{II} phthalocyanine (FePc), a planar-shaped molecular complex. It is of note that FePc does not leach out Fe cations in acidic medium as long as it is at open circuit potential (OCP),[46] which is the condition employed during our H_2O_2 treatment. Recently, it was clearly shown that demetalation of FePc in acidic medium requires electrochemical polarization to low potential.[46] With such a model compound for FeN_4 sites with high accessibility, the ROS formed by reaction between FeN_4 and H_2O_2 should easily be trapped by DMPO. The EPR spectrum obtained from FePc showed an approximately six-fold stronger signal of •DMPO-OH spin adduct at pH 2, compared with that obtained from FeNC-dry-0.5 (Figure 5a). The quartet signal was also detected at pH 4 and 6 (Figure 5b), but with much lower intensity.
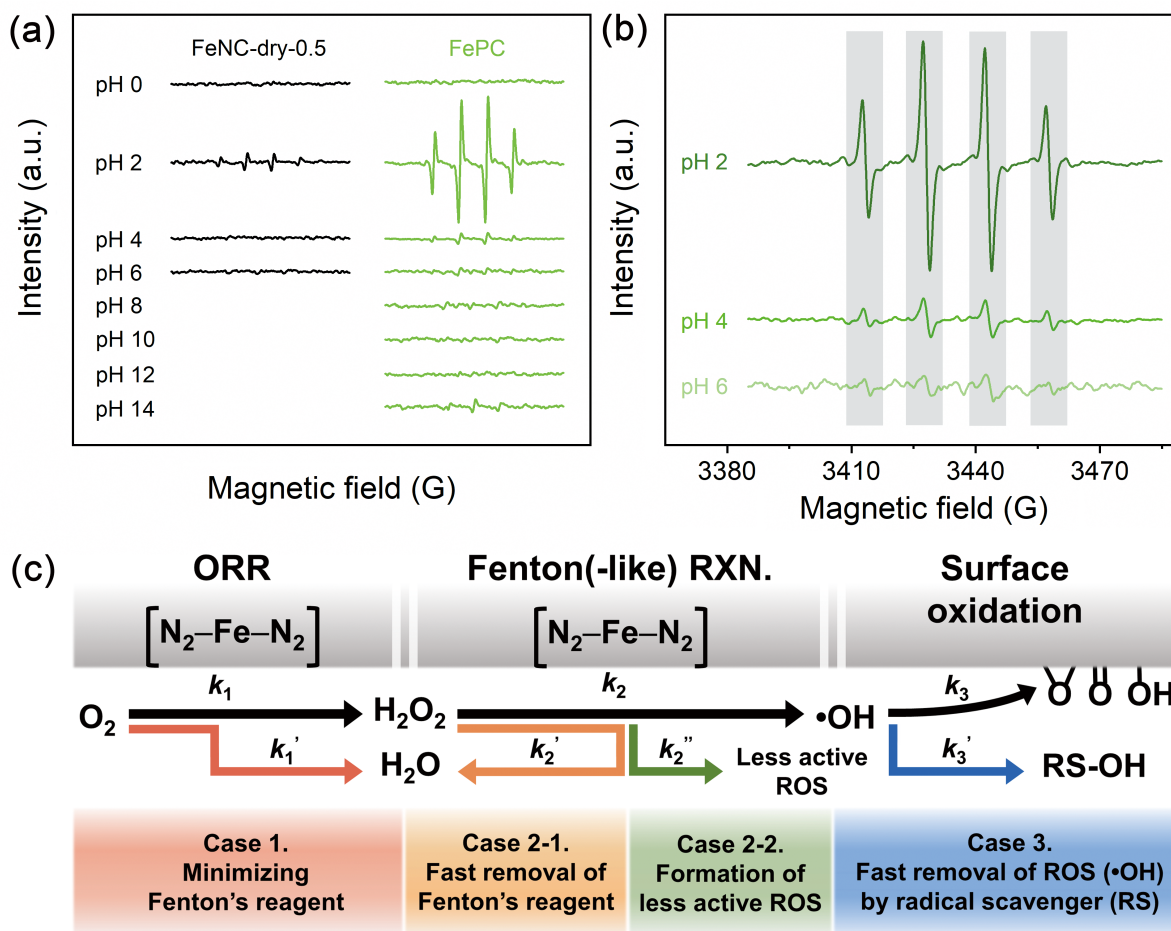
Figure 5. (a) Comparison of EPR spectra measured for FeNC-dry-0.5 and FePc in H_2O_2-containing solution pH range of 0–6 and 0–14, respectively. With FeNC-dry-0.5, the •DMPO-OH adduct signal was distinguishable only at pH 2, while a nearly six-fold stronger signal was obtained for FePc at the same pH. (b) Magnified EPR spectra obtained at pH 2, 4, and 6 with FePc. The main quartet signal characteristic for the •DMPO-OH adduct is indicated by the gray-colored columns. (c) Outline of deactivation mechanism of Fe-N-C catalysts induced by H_2O_2 and suggested synthetic/system-level strategies to bypass the deactivation pathway. The deactivation mechanism consisted of consecutive ORR, Fenton(-like) reaction, and surface oxidation steps. The k_n (n = 1–3) parameters are the rate constants of the respective deactivation steps, while k_n' and k_n" denote those of the bypassing reactions.

From the similar trends seen between the extent of deactivation of FeNC-dry-0.5 after H_2O_2 treatment at pH 0, 2, 4, or 6 and the quartet intensity identified in the EPR spectra (Figures 2 and 5, respectively), one can conclude that the ROS formed by Fenton(-like) reactions is likely to be a key deactivating agent of Fe-N-C catalysts. It is however not possible to conclude which ROS is formed, due to fast decomposition of all •DMPO-ROS adducts into the •DMPO-OH adduct.[21] Nevertheless, considering the much stronger oxidizing ability of the hydroxyl radical

15

($E^0 = 2.33$ V$_{SHE}$ at pH 7) compared to that of other ROS ($E^0 = 1.06$ and 0.94 V$_{SHE}$ for hydroperoxyl and superoxide radicals, respectively),[47] the hydroxyl radical can be assigned as the most detrimental ROS for Fe-N-C catalysts. This conclusion is consistent with the literature,[48-50] although previous works mainly focused on the PEM/ionomer degradation at the Pt/C cathode during PEMFC operation.

Based on the drawn conclusion, new directions could be proposed for the synthesis of next-generation Fe-N-C catalysts with improved durability in PEMFCs (Figure 5c). It is of note that a mitigation of the H_2O_2-induced deactivation path should be accomplished to achieve the durable operation of PEMFCs even for highly selective (low H_2O_2 formation at initial stage) Fe-N-C catalysts. The reason is that this deactivation process is an evil circle, with trace amount of H_2O_2 at beginning-of-life oxidizing the Fe-N-C surface, leading to progressively increased H_2O_2 formation during ORR as a function of time, leading in turn to accelerated deactivation *via* Fenton process. The synthesis of Fe-N-C catalysts with very low H_2O_2 production at beginning-of-life is therefore insufficient to solve this deactivation issue, and lower H_2O_2 production should be maintained during operation. The chemical deactivation mechanism can be divided into three consecutive steps: ORR, Fenton(-like) reaction, and surface oxidation. Therefore, prolonged PEMFC operation would be possible by controlling the reaction selectivity or by minimizing the formation of ROS. Namely, achieving enhanced selectivity at the atomic scale (*i.e.*, on the active sites, not as a result of 2+2 or 2×2 pathways) for the direct four-electron ORR pathway can be considered as a primary goal to minimize the downstream production of ROS from H_2O_2 ($k_1 \ll k_1$', case 1 in Figure 5c).[51-52] On the other hand, ROS formation could be minimized by the introduction of secondary catalytic sites at which H_2O_2 is electrochemically reduced or decomposed to H_2O at a much faster rate compared to the Fenton(-like) reaction on Fe moieties ($k_2 \ll k_2$', case 2-1 in Figure 5c).[53-55] Replacing Fe-based

16

active sites by active sites comprising other transition metals (*e.g.*, Co and Mn) could also be a good strategy to mitigate the deactivation of metal-N-C (Me-N-C) catalysts during operation, due to the generally accepted view (although not clearly demonstrated yet) that other 3d metal cations may have milder Fenton reactivity compared to Fe cations.[56-58]

Besides the synthetic strategies proposed above for preparing or modifying Fe-N-C and Me-N-C catalysts with improved durability in operation, this study provides further insight into how the systematic replacement of acidic PEM electrolytes by anion-exchange membrane (AEM) electrolytes not only leads to a broader set of platinum-group metal (PGM)-free ORR catalysts and enhanced ORR activity of Fe-N-C catalysts, but should also lead to a much enhanced durability of Fe-N-C catalysts, and maybe other classes of ORR catalysts as well. It is of note that a Fe-N-C catalyst very similar to the one studied in the present work achieved a peak power density of 1.44 W cm^{-2} in H$_2$/O$_2$ AEMFC, exceeding the best power performance compared to any other AEMFCs with PGM-free cathodes.[59] In addition, it is expected that enhanced durability is based on the absence or benign effect of Fenton(-like) reactions at high pH, observed in this work on Fe-N-C. This dramatic pH change from PEM to AEM environment can effectively alter the selectivity of the Fenton(-like) reactions, limiting the formation of very harmful ROS such as the hydroxyl radical ($k_2 \ll k_2$", case 2-2 in Figure 5c). This expected improved durability of PGM-free ORR catalysts in AEMFC is in line with recent results showing promising durability of different types of catalysts based on 3d transition metals in operating AEMFCs.[60-63] Their operational durability is comparable with (or even better than) that of commercial Pt/C catalysts.[59] However, at present, some technical issues associated with other components (*e.g.*, instability of the AEMs in low relative humidity conditions, rather than of the catalysts) remain as critical hurdles for the implementation of AEMFCs, as well as carbonation problems when ambient air is used.[64-66]

17
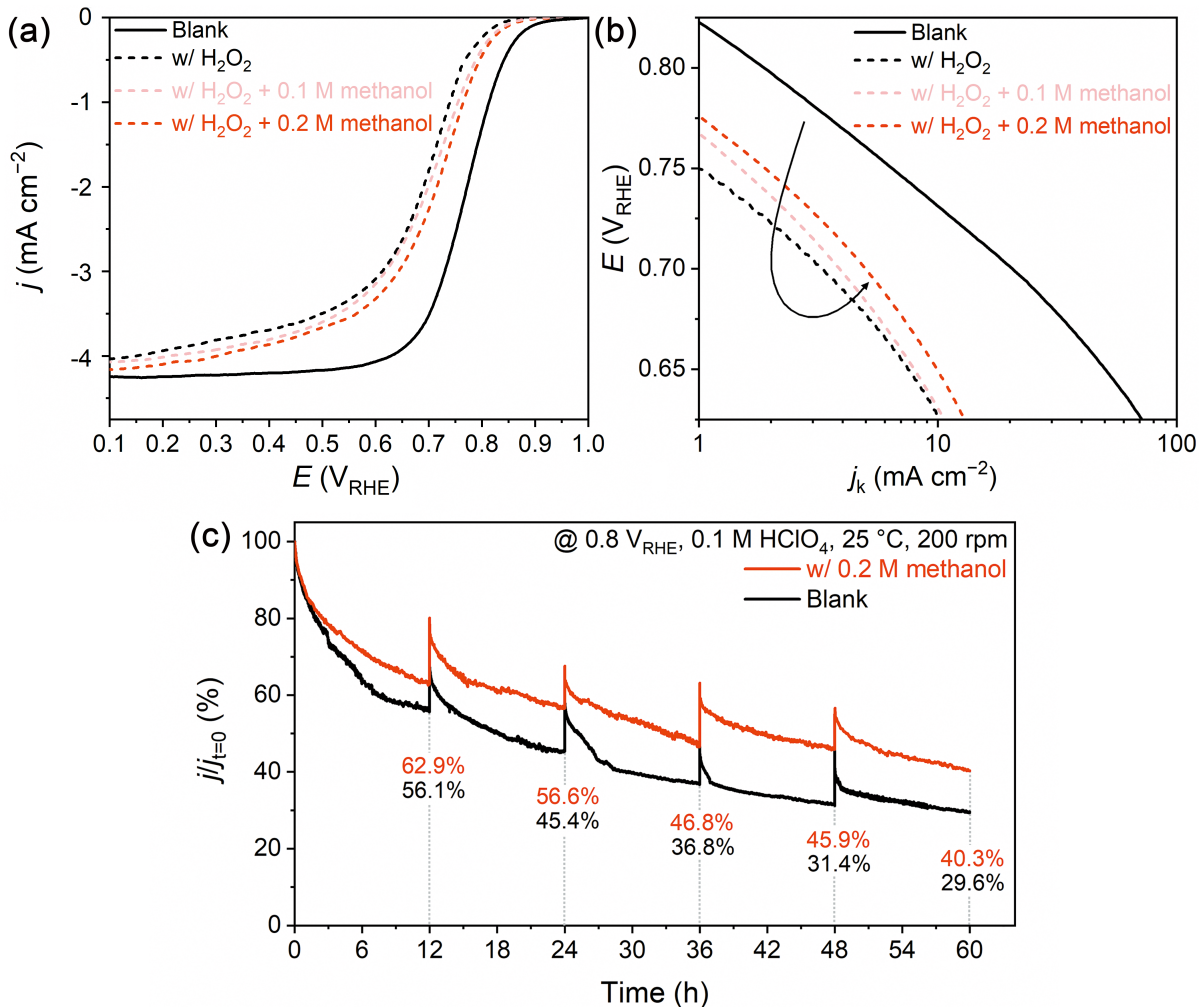
Figure 6. Experimental demonstration of homogeneous radical scavenging strategy with methanol. (a) ORR polarization curves measured before and after the H_2O_2 treatment in an acidic condition (pH 1) and (b) corresponding Tafel plots. During the H_2O_2 treatment, 0.1 or 0.2 M methanol was introduced to the treatment solution. (c) Normalized current density of the FeNC-dry-0.5 catalytic layer as a function of time. The catalytic layer was polarized at a constant potential of 0.8 V_{RHE} for 60 h in the presence or absence of 0.2 M methanol in an O_2-saturated 0.1 M $HClO_4$ electrolyte.

Otherwise, durable Fe-N-C electrocatalysts in PEMFCs could also be attained by avoiding the surface oxidation step (*i.e.*, the third step in the deactivation mechanism). This could be achieved by introducing suitable radical scavengers near the Fe-based sites that rapidly react with the ROS (hydroxyl radical in particular) ($k_3 \ll k_3$', case 3 in Figure 5c). As a synthetic approach, this strategy has been well exemplified with the addition of CeO_2 in Pt-based PEMFCs in order to extend the durability of PEMs.[67-68] However, for Fe-N-C catalysts, this

18

strategy has not resulted in highly improved durability yet, probably due to a lack of efficient radical scavengers working in micropores, where the most active FeN_x sites are located. Hence, to evaluate the feasibility of the radical scavenging strategy to stabilize Fe-N-C, we considered a "homogeneous" radical scavenger, namely methanol, with greater accessibility to FeN_x sites than ceria or zirconia nanoparticles and its comparable ROS scavenging activity.[69] ORR polarization curves measured before and after the H_2O_2 treatment (at pH 1) showed that the activity loss of FeNC-dry-0.5 was mitigated by the presence of methanol, and decreased with increasing methanol concentration (Figures 6a and b). Durability test at a constant potential of 0.8 V_{RHE}, almost identical protocol used for aforementioned Co-N-C and Mn-N-C catalysts,[57-58] showed that ORR activity decay was *ca.* −70% in the methanol-free electrolyte (blank) but it was reduced to *ca.* −60% with 0.2 M methanol after 60 h operation (Figure 6c). The $\Delta E_{1/2}$ value, measured before and after the durability test, was also reduced in the presence of methanol (*i.e.,* $\Delta E_{1/2}$ = −73 and −43 mV in the absence and presence of 0.2 M methanol, respectively; Figure S7). While this strategy could not be optimized at the moment, the result gives a first sign that an optimized radical scavenging strategy might be effective in the near future to improve the durability of Fe-N-C catalysts in PEMFC systems.

CONCLUSION

In summary, the ORR deactivation of Fe-N-C catalyst induced by H_2O_2 was investigated at various pH conditions. Acidic H_2O_2 treatments resulted in a severe activity drop, correlated with partial oxidation of the catalyst surface. The maximum deactivation was observed at pH 2. For pH values > 2, the deactivation extent was continuously reduced with increasing pH of the H_2O_2 treatment solution. EPR results indicated that the concentration of •DMPO-OH spin adduct produced by the Fenton(-like) reactions correlated well with the deactivation trends, allowing us to conclude that the ROS play a key role in the deactivation of Fe-N-C. This finding opens

up new avenues for the development of durable Fe-N-C catalysts in fuel cells *via* rational

mitigation strategies countering the deactivation mechanism, either at the catalyst or system

level. In particular, two main lines of research are identified for replacing PGM-based cathodes

in low-temperature fuel cells, one leaning on modified Me-N-C cathodes in the acidic medium

of PEMFCs and another one leaning on a drastically increased pH environment by switching

from PEM to AEM electrolyte. In the latter case however, other challenges must be overcome

before industrial application of AEMFC, such as *operando* AEM stability and carbonation

issue.[70] On the other hand, minimization of Fenton's reagents (*i.e.*, H_2O_2) and fast scavenging of

ROS formed near the FeN_x sites can be considered as rational strategies to improve the

durability of Fe-N-C and other Me-N-C catalysts in acidic PEMFC.

EXPERIMENTAL SECTION

Catalysts Synthesis and H_2O_2 Treatment. The FeNC-dry-0.5 catalyst was synthesized *via* the

same method used in our previous studies.[21, 25] Fe^{II} acetate, 1,10-phenanthroline, and ZIF-8

($ZnN_4C_8H_{12}$, Basolite Z1200 from Aldrich) precursors were directly mixed by a dry ball-milling

(FRITSCH Pulverisette 7 Premium) for four cycles of 30 min at 400 rpm. A ZrO_2 crucible with

100 zirconium oxide balls of 5 mm diameter was used in this procedure. The precursor powder

contained 0.5 wt.% Fe and the mass ratio of 1,10-phenanthroline to ZIF-8 was 20:80. The

resulting powder was then pyrolyzed at 1050 °C under Ar flow for 1 h.

The H_2O_2 treatment was performed in a pH-adjusted solution containing 1 wt.% H_2O_2,

referred to as 'oxidizing solution' in the following. For electrochemical characterization

purposes, the catalytic layer (loading 800 μg cm^{-2}) comprising FeNC-dry-0.5 deposited on a

glassy carbon tip (3 mm diameter) was immersed in the oxidizing solution for 2 h. The

electrode was rotated at 2,500 rpm to remove O_2 bubbles formed from H_2O_2 disproportionation,

and kept at OCP. Temperature was maintained at 50 °C by a bath circulator (RW3-0525, Lab

Companion). H_2O_2 concentration during the treatment was measured by an iodometry titration

method with KI (99%, Aldrich), $(NH_4)_6Mo_7O_{24} \cdot 4H_2O$ (81–83%, Aldrich), H_2SO_4 (95–98%,

Aldrich), $Na_2S_2O_3$ (98%, Aldrich), and starch indicator (2%, Aldrich).[71] The pH-adjusted

oxidizing solutions were prepared using concentrated $HClO_4$ (70%, Aldrich) for pH 0–2, H_3PO_4

(85%, Aldrich) for pH 3–8, $KHCO_3$ (99.7%, Aldrich) for pH 9–12, and KOH pellet (90%,

Aldrich) for pH 13–14, respectively. The pH of the solutions was experimentally measured

with a pH meter (HM-30P, TOADKK) under N_2 bubbling. For physical characterization

purposes, the H_2O_2 treatment was performed with 0.12 g of FeNC-dry-0.5 dispersed into 600

mL of the oxidizing solutions at 50 °C, whose pH was adjusted as 1, 7, or 13. After 2 h, the

catalyst powder was collected by filtration, washed with 1 L ultrapure water, and dried at 80

°C overnight.

Electrochemical Characterizations. Electrochemical properties were investigated with a

VMP-300 potentiostat (Bio-Logic) in a three-electrode cell equipped with a graphite rod as a

counter electrode and a saturated Ag/AgCl as a reference electrode (EC-Frontier). A 0.1 M

$HClO_4$ electrolyte was prepared with ultrapure water (> 18 MΩ, Sartorious) and concentrated

$HClO_4$. All potentials noted in this study are referenced to the reversible hydrogen electrode

(RHE), after calibration of the reference electrode in the H_2-saturated electrolyte with a Pt

electrode. A FeNC-dry-0.5 ink was prepared by dispersing 10 mg catalyst in 884 μL ink

solution [804 μL water, 80 μL Nafion solution (5 wt.%)]. The working electrode was fabricated

by dropping the catalyst ink (5 μL) onto the glassy carbon (0.07 cm^2) of the RDE (01169, ALS

Co.), and then left for drying at room temperature. The catalyst loading was set to 800 μg cm^{-2}.

The ORR polarization curves were recorded with a scan rate of 10 mV s^{-1} and a rotation speed

of 900 rpm in the O_2-saturated electrolyte. ORR Faradaic currents were obtained by

substracting the polarization curves measured in N_2-saturated electrolyte. RRDE analysis was carried out using a RRDE electrode (012613, ALS) equipped with a Pt ring. The Pt ring electrode was polarized at a constant potential of 1.2 V_{RHE} during the ORR polarization on the disk electrode. The collection efficiency of 0.385 was used after $Fe^{2+/3+}$ redox calibration. Durability test was conducted by holding at a constant potential of 0.8 V_{RHE} for 60 h with a 200 rpm rotation speed, in the presence and absence of 0.2 M methanol in the electrolte. During the durability test, the electrode was treated by 30 potential cyclings between 0 to 1.0 V_{RHE} every 12 h.

Physico-chemical Characterizations. The Fourier transforms of the EXAFS signal was obtained from Fe K-edge X-ray absorption spectrum at the SAMBA beamline (Synchrotron SOLEIL). The catalyst was pelletized with a Teflon powder binder. The ^{57}Fe Mössbauer spectrum was acquired with a source of ^{57}Co in Rh. The measurement was performed keeping both the source and the absorber at room temperature. The spectrometer was operated with a triangular velocity waveform, and a NaI scintillation detector was used for detecting the γ-rays. XRD patterns were obtained with a high resolution powder X-ray diffractometer (Dmax2500, Rikaku) equipped with a Cu K_α X-ray source. The XRD patterns were measured at an accelerating voltage of 45 kV and a current of 200 mA, with a scan rate of 5° min^{-1} and a step size of 0.01°. Raman spectra were obtained by a LabRAM HR (HORIBA) spectrometer with 514 nm laser excitation. N_2 adsorption-desorption isotherms were measured using a BEL-SOPR-max (BEL Japan) volumetric analyzer at −196 °C. Before each measurement, the sample was degassed at 200 °C for 4 h. XPS measurements were carried out using a Sigma Probe (Thermo VG Scientific) instrument equipped with a microfocused monochromator X-ray source. ICP-MS was performed using a Polyscan 61E (Hewlett-Packard), for determining

the Fe content of the samples. Elemental analysis was carried out using a Flash 2000 series (Thermo Scientific) instrument.

E_{pzc} was measured by staircase potentiostatic electrochemical impedance spectroscopy in a VMP3 potentiostat (Biologic). Scans were carried out in the potential range of -1.5 to 0.5 $V_{Ag/AgCl}$ at a 100 mHz frequency, with 10 mV amplitude in a 2 mM NaF solution. E_{pzc} was defined as the potential at the minimum capacitance of the electrochemical double layer. ΔpH_f was determined by measuring the pH change of the corresponding solutions after the catalysts were dispersed. Under N_2 bubbling, 40 mg of catalyst was dispersed in 30 mL of pH 6 solution, prepared from a mixture of 0.1 M H_2SO_4 and 0.1 M KOH solutions. The pH was recorded as a function of time before and after introduction of the catalyst powder in solution, and the stationary pH value after the addition of catalyst (pH_f) was recorded. To compare pristine FeNC-dry-0.5 and H_2O_2-treated catalysts, the change in acido-basicity was expressed as ΔpH_f = pH_f (after H_2O_2 treatment at a given pH) $-$ pH_f (pristine catalyst). A negative ΔpH_f value indicates an acidification of the surface relative to the pristine catalyst.

EPR measurements were conducted on a Bruker EMX/plus spectrometer equipped with a dual mode cavity (ER 4116DM). The experimental conditions were set as follows: 9.64 GHz microwave frequency, 10 G modulation amplitude, 100 kHz modulation frequency, 0.94 mW microwave power, and 25 °C temperature. Ten scans were accumulated for each spectrum. EPR aliquot samples were prepared as follows: first, 1.80 mg of FeNC-dry-0.5 (or 0.25 mg of FePc; their Fe amount was identical to 0.027 mg) was dispersed in pH-adjusted solution. After 30 min of sonication, the desired amounts of DMPO (> 98%, Aldrich) and H_2O_2 were sequentially added to reach the concentrations of 0.4 M and 0.5 wt.%, respectively. The resulting total volume of the solution was 0.5 mL. After 5 min reaction, the solution was filtered

(syringe polypropylene filter, 0.2 μm, Whatman) to separate the catalyst powder from the liquid

aliquot, which was subsequently examined by EPR.

AUTHOR INFORMATION

Corresponding Author

*E-mail: chchoi@gist.ac.kr (C.H.C.)

*E-mail: frederic.jaouen@umontpellier.fr (F.J.)

Author Contributions

C.H.C. and F.J. designed the research. G.S.B., M.W.C., and S.G.J. performed the experiments. The manuscript was written through contributions of all authors. §These authors contributed equally.

ASSOCIATED CONTENT

Supporting Information

The following file is available free of charge.

Additional physical/electrochemical characterization data: EXAFS, [57]Fe Mössbauer spectrum, XRD patterns, Raman spectra, N_2 adsorption isotherms, compositions measured by elemental analysis, H_2O_2 concentration profile, RRDE results, correlation curves between j_k and E_{PZC} or ΔpH_1, and ORR polarization curves before and after the durability test (PDF)

REFERENCES

1.   Chung, H. T.; Cullen, D. A.; Higgins, D.; Sneed, B. T.; Holby, E. F.; More, K. L.; Zelenay, P., Direct Atomic-Level Insight into the Active Sites of A High-Performance PGM-Free ORR Catalyst. *Science* **2017,** 357, 479-484.

2.   Lefèvre, M.; Proietti, E.; Jaouen, F.; Dodelet, J.-P., Iron-Based Catalysts with Improved Oxygen Reduction Activity in Polymer Electrolyte Fuel Cells. *Science* **2009,** 324, 71-74.

3.   Wu, G.; More, K. L.; Johnston, C. M.; Zelenay, P., High-Performance Electrocatalysts for Oxygen Reduction Derived from Polyaniline, Iron, and Cobalt. *Science* **2011,** 332, 443-447.

4.   Chen, Z.; Higgins, D.; Yu, A.; Zhang, L.; Zhang, J., A Review on Non-Precious Metal Electrocatalysts for PEM Fuel Cells. *Energy Environ. Sci.* **2011,** 4, 3167-3192.

5.   Proietti, E.; Jaouen, F.; Lefèvre, M.; Larouche, N.; Tian, J.; Herranz, J.; Dodelet, J.-P., Iron-Based Cathode Catalyst with Enhanced Power Density in Polymer Electrolyte Membrane Fuel Cells. *Nat. Commun.* **2011,** 2, 416.

6.   Li, Y.; Zhou, W.; Wang, H.; Xie, L.; Liang, Y.; Wei, F.; Idrobo, J.-C.; Pennycook, S. J.; Dai, H., An Oxygen Reduction Electrocatalyst Based on Carbon Nanotube–Graphene Complexes. *Nat. Nanotechnol.* **2012,** 7, 394-400.

7.   Wang, W.; Jia, Q.; Mukerjee, S.; Chen, S., Recent Insights into the Oxygen-Reduction Electrocatalysis of Fe/N/C Materials. *ACS Catal.* **2019,** 9, 10126-10141.

8.   Li, J.; Zhang, H.; Samarakoon, W.; Shan, W.; Cullen, D. A.; Karakalos, S.; Chen, M.; Gu, D.; More, K. L.; Wang, G.; Feng, Z.; Wang, Z.; Wu, G., Thermally Driven Structure and Performance Evolution of Atomically Dispersed FeN_4 Sites for Oxygen Reduction. *Angew. Chem. Int. Ed.* **2019,** 58, 18971-18980.

9.   Zhang, H.; Chung, H. T.; Cullen, D. A.; Wagner, S.; Kramm, U. I.; More, K. L.; Zelenay, P.; Wu, G., High-Performance Fuel Cell Cathodes Exclusively Containing Atomically Dispersed Iron Active Sites. *Energy Environ. Sci.* **2019,** 12, 2548-2558.

10.   Banham, D.; Ye, S.; Pei, K.; Ozaki, J.-i.; Kishimoto, T.; Imashiro, Y., A Review of the Stability and Durability of Non-Precious Metal Catalysts for the Oxygen Reduction Reaction in Proton Exchange Membrane Fuel Cells. *J. Power Sources* **2015,** 285, 334-348.

11.   Shao, M.; Chang, Q.; Dodelet, J.-P.; Chenitz, R., Recent Advances in Electrocatalysts for Oxygen Reduction Reaction. *Chem. Rev.* **2016,** 116, 3594-3657.

12.   Choi, C. H.; Baldizzone, C.; Polymeros, G.; Pizzutilo, E.; Kasian, O.; Schuppert, A. K.; Ranjbar Sahraie, N.; Sougrati, M.-T.; Mayrhofer, K. J. J.; Jaouen, F., Minimizing Operando Demetallation of Fe-N-C Electrocatalysts in Acidic Medium. *ACS Catal.* **2016,** 6, 3136-3146.

13.   Chenitz, R.; Kramm, U. I.; Lefèvre, M.; Glibin, V.; Zhang, G.; Sun, S.; Dodelet, J.-P., A Specific Demetalation of Fe–N_4 Catalytic Sites in the Micropores of NC_Ar + NH_3 is at the Origin of the Initial Activity Loss of the Highly Active Fe/N/C Catalyst Used for the Reduction of Oxygen in PEM Fuel Cells. *Energy Environ. Sci.* **2018,** 11, 365-382.

14.   Zhang, G.; Chenitz, R.; Lefèvre, M.; Sun, S.; Dodelet, J.-P., Is Iron Involved in the Lack of Stability of Fe/N/C Electrocatalysts Used to Reduce Oxygen at the Cathode of PEM Fuel Cells? *Nano Energy* **2016,** 29, 111-125.

15.   Ferrandon, M.; Wang, X.; Kropf, A. J.; Myers, D. J.; Wu, G.; Johnston, C. M.; Zelenay, P., Stability of Ion Species in Heat-Treated Polyaniline–Iron–Carbon Polymer Electrolyte Fuel Cell Cathode Catalysts. *Electrochim. Acta* **2013,** 110, 282-291.

16.   Herranz, J.; Jaouen, F.; Lefèvre, M.; Kramm, U. I.; Proietti, E.; Dodelet, J.-P.; Bogdanoff, P.; Fiechter, S.; Abs-Wurmbach, I.; Bertrand, P.; Arruda, T. M.; Mukerjee, S., Unveiling N-Protonation and Anion-Binding Effects on Fe/N/C Catalysts for O_2 Reduction in Proton-Exchange-Membrane Fuel Cells. *J. Phys. Chem. C* **2011,** 115, 16087-16097.

17.   Goellner, V.; Baldizzone, C.; Schuppert, A.; Sougrati, M. T.; Mayrhofer, K.; Jaouen, F., Degradation of Fe/N/C Catalysts Upon High Polarization in Acid Medium. *Phys. Chem. Chem. Phys.* **2014,** 16, 18454-18462.

18.   Goellner, V.; Armel, V.; Zitolo, A.; Fonda, E.; Jaouen, F., Degradation by Hydrogen Peroxide of Metal-Nitrogen-Carbon Catalysts for Oxygen Reduction. *J. Electrochem. Soc.* **2015,** 162, H403-H414.

19.   Lefèvre, M.; Dodelet, J.-P., Fe-Based Catalysts for the Reduction of Oxygen in Polymer Electrolyte Membrane Fuel Cell Conditions: Determination of the Amount of Peroxide Released during Electroreduction and Its Influence on the Stability of the Catalysts. *Electrochim. Acta* **2003,** 48, 2749-2760.

20.   Wu, G.; Artyushkova, K.; Ferrandon, M.; Kropf, A. J.; Myers, D.; Zelenay, P., Performance Durability of Polyaniline-Derived Non-Precious Cathode Catalysts. *ECS Trans.* **2009,** 25, 1299-1311.

21.   Choi, C. H.; Lim, H.-K.; Chung, M. W.; Chon, G.; Ranjbar Sahraie, N.; Altin, A.; Sougrati, M.-T.; Stievano, L.; Oh, H. S.; Park, E. S.; Luo, F.; Strasser, P.; Dražić, G.; Mayrhofer, K. J. J.; Kim, H.; Jaouen, F., The Achilles' Heel of Iron-Based Catalysts during Oxygen Reduction in An Acidic Medium. *Energy Environ. Sci.* **2018,** 11, 3176-3182.

22.   Yin, X.; Zelenay, P., Kinetic Models for the Degradation Mechanisms of PGM-Free ORR Catalysts. *ECS Trans.* **2018,** 85, 1239-1250.

23.   Möller, S.; Barwe, S.; Masa, J.; Wintrich, D.; Seisel, S.; Baltruschat, H.; Schuhmann, W., Online Monitoring of Electrochemical Carbon Corrosion in Alkaline Electrolytes by Differential Electrochemical Mass Spectrometry. *Angew. Chem. Int. Ed.* **2020,** 59, 1585-1589.

24.   Zitolo, A.; Goellner, V.; Armel, V.; Sougrati, M.-T.; Mineva, T.; Stievano, L.; Fonda, E.; Jaouen, F., Identification of Catalytic Sites for Oxygen Reduction in Iron- and Nitrogen-Doped Graphene Materials. *Nat. Mater.* **2015,** 14, 937-942.

25. Chung, M. W.; Chon, G.; Kim, H.; Jaouen, F.; Choi, C. H., Electrochemical Evidence for Two Sub-Families of FeN_xC_y Moieties with Concentration-Dependent Cyanide Poisoning. *ChemElectroChem* **2018,** 5, 1880-1885.

26. Ramaswamy, N.; Mukerjee, S., Influence of Inner- and Outer-Sphere Electron Transfer Mechanisms during Electrocatalysis of Oxygen Reduction in Alkaline Media. *J. Phys. Chem. C* **2011,** 115, 18015-18026.

27. Bard, A. J.; Faulkner, L. R., *Electrochemical Methods: Fundamentals and Applications*. 2nd ed.; Wiley: New York, 2001; pp 92.

28. Nidheesh, P. V., Heterogeneous Fenton Catalysts for the Abatement of Organic Pollutants From Aqueous Solution: A Review. *RSC Adv.* **2015,** 5, 40552-40577.

29. Dutta, K.; Bhattacharjee, S.; Chaudhuri, B.; Mukhopadhyay, S., Chemical Oxidation of C. I. Reactive Red 2 using Fenton-Like Reactions. *J. Environ. Monit.* **2002,** 4, 754-760.

30. Seger, B.; Vinodgopal, K.; Kamat, P. V., Proton Activity in Nafion Films: Probing Exchangeable Protons with Methylene Blue. *Langmuir* **2007,** 23, 5471-5476.

31. Yang, K.; Kas, R.; Smith, W. A., *In Situ* Infrared Spectroscopy Reveals Persistent Alkalinity near Electrode Surfaces during CO_2 Electroreduction. *J. Am. Chem. Soc.* **2019,** 141, 15891-15900.

32. Eslamibidgoli, M. J.; Huang, J.; Kadyk, T.; Malek, A.; Eikerling, M., How Theory and Simulation Can Drive Fuel Cell Electrocatalysis. *Nano Energy* **2016,** 29, 334-361.

33. Jung, E.; Shin, H.; Lee, B.-H.; Efremov, V.; Lee, S.; Lee, H. S.; Kim, J.; Hooch Antink, W.; Park, S.; Lee, K.-S.; Cho, S.-P.; Yoo, J. S.; Sung, Y.-E.; Hyeon, T., Atomic-Level Tuning of Co–N–C Catalyst for High-Performance Electrochemical H_2O_2 Production. *Nat. Mater.* **2020,** 19, 436-442.

34. Emets, V. V.; Damaskin, B. B., The Relation between the Potential of Zero Charge and Work Function for sp-Metals. *Russ. J. Electrochem.* **2009,** 45, 45-57.

35.   Jung, Y. S.; Lim, W. T.; Park, J. Y.; Kim, Y. H., Effect of pH on Fenton and Fenton-Like Oxidation. *Environ. Technol.* **2009,** 30, 183-190.

36.   Gallard, H.; De Laat, J., Kinetic Modelling of Fe(III)/H_2O_2 Oxidation Reactions in Dilute Aqueous Solution using Atrazine as A Model Organic Compound. *Water Res.* **2000,** 34, 3107-3116.

37.   Pesterfield, L. L.; Maddox, J. B.; Crocker, M. S.; Schweitzer, G. K., Pourbaix (E–pH-M) Diagrams in Three Dimensions. *J. Chem. Educ.* **2012,** 89, 891-899.

38.   Copéret, C.; Chabanas, M.; Petroff Saint-Arroman, R.; Basset, J.-M., Homogeneous and Heterogeneous Catalysis: Bridging the Gap through Surface Organometallic Chemistry. *Angew. Chem. Int. Ed.* **2003,** 42, 156-181.

39.   Lu, H.-F.; Chen, H.-F.; Kao, C.-L.; Chao, I.; Chen, H.-Y., A Computational Study of the Fenton Reaction in Different pH Ranges. *Phys. Chem. Chem. Phys.* **2018,** 20, 22890-22901.

40.   Bataineh, H.; Pestovsky, O.; Bakac, A., pH-Induced Mechanistic Changeover From Hydroxyl Radicals to Iron(IV) in the Fenton Reaction. *Chem. Sci.* **2012,** 3, 1594-1599.

41.   Duesterberg, C. K.; Mylon, S. E.; Waite, T. D., pH Effects on Iron-Catalyzed Oxidation using Fenton's Reagent. *Environ. Sci. Technol.* **2008,** 42, 8522-8527.

42.   Hug, S. J.; Leupin, O., Iron-Catalyzed Oxidation of Arsenic(III) by Oxygen and by Hydrogen Peroxide: pH-Dependent Formation of Oxidants in the Fenton Reaction. *Environ. Sci. Technol.* **2003,** 37, 2734-2742.

43.   Choi, C. H.; Baldizzone, C.; Grote, J.-P.; Schuppert, A. K.; Jaouen, F.; Mayrhofer, K. J. J., Stability of Fe-N-C Catalysts in Acidic Medium Studied by Operando Spectroscopy. *Angew. Chem. Int. Ed.* **2015,** 54, 12753-12757.

44.   Santori, P. G.; Speck, F. D.; Li, J.; Zitolo, A.; Jia, Q.; Mukerjee, S.; Cherevko, S.; Jaouen, F., Effect of Pyrolysis Atmosphere and Electrolyte pH on the Oxygen Reduction

Activity, Stability and Spectroscopic Signature of FeN_x Moieties in Fe-N-C Catalysts. *J. Electrochem. Soc.* **2019,** 166, F3311-F3320.

45.   Buettner, G. R., The spin trapping of superoxide and hydroxyl free radicals with DMPO (5,5-dimethylpyrroline-N-oxide): more about iron. *Free Radic. Res. commun.* **1993,** 19 Suppl 1, S79-S87.

46.   Chen, Z.; Jiang, S.; Kang, G.; Nguyen, D.; Schatz, G. C.; Van Duyne, R. P., Operando Characterization of Iron Phthalocyanine Deactivation during Oxygen Reduction Reaction Using Electrochemical Tip-Enhanced Raman Spectroscopy. *J. Am. Chem. Soc.* **2019,** 141, 15684-15692.

47.   Buettner, G. R., The Pecking Order of Free Radicals and Antioxidants: Lipid Peroxidation, α-Tocopherol, and Ascorbate. *Arch. Biochem. Biophys.* **1993,** 300, 535-543.

48.   Bi, W.; Gray, G. E.; Fuller, T. F., PEM Fuel Cell Pt/C Dissolution and Deposition in Nafion Electrolyte. *Electrochem. Solid-State Lett.* **2007,** 10, B101-B104.

49.   Panchenko, A.; Dilger, H.; Kerres, J.; Hein, M.; Ullrich, A.; Kaz, T.; Roduner, E., *In-Situ* Spin Trap Electron Paramagnetic Resonance Study of Fuel Cell Processes. *Phys. Chem. Chem. Phys.* **2004,** 6, 2891-2894.

50.   Endoh, E.; Terazono, S.; Widjaja, H.; Takimoto, Y., Degradation Study of MEA for PEMFCs under Low Humidity Conditions. *Electrochem. Solid-State Lett.* **2004,** 7, A209.

51.   Choi, C. H.; Choi, W. S.; Kasian, O.; Mechler, A. K.; Sougrati, M. T.; Brüller, S.; Strickland, K.; Jia, Q.; Mukerjee, S.; Mayrhofer, K. J. J.; Jaouen, F., Unraveling the Nature of Sites Active toward Hydrogen Peroxide Reduction in Fe-N-C Catalysts. *Angew. Chem. Int. Ed.* **2017,** 56, 8809-8812.

52.   Sa, Y. J.; Park, S. O.; Jung, G. Y.; Shin, T. J.; Jeong, H. Y.; Kwak, S. K.; Joo, S. H., Heterogeneous Co–N/C Electrocatalysts with Controlled Cobalt Site Densities for the

Hydrogen Evolution Reaction: Structure–Activity Correlations and Kinetic Insights. *ACS Catal.* **2019,** 9, 83-97.

53.   Chong, L.; Wen, J.; Kubal, J.; Sen, F. G.; Zou, J.; Greeley, J.; Chan, M.; Barkholtz, H.; Ding, W.; Liu, D.-J., Ultralow-Loading Platinum-Cobalt Fuel Cell Catalysts Derived From Imidazolate Frameworks. *Science* **2018,** 362, 1276-1281.

54.   Shao, Y.; Dodelet, J.-P.; Wu, G.; Zelenay, P., PGM-Free Cathode Catalysts for PEM Fuel Cells: A Mini-Review on Stability Challenges. *Adv. Mater.* **2019,** 31, 1807615.

55.   Mechler, A. K.; Sahraie, N. R.; Armel, V.; Zitolo, A.; Sougrati, M. T.; Schwämmlein, J. N.; Jones, D. J.; Jaouen, F., Stabilization of Iron-Based Fuel Cell Catalysts by Non-Catalytic Platinum. *J. Electrochem. Soc.* **2018,** 165, F1084-F1091.

56.   Wang, X. X.; Prabhakaran, V.; He, Y.; Shao, Y.; Wu, G., Iron-Free Cathode Catalysts for Proton-Exchange-Membrane Fuel Cells: Cobalt Catalysts and the Peroxide Mitigation Approach. *Adv. Mater.* **2019,** 31, 1805126.

57.   Li, J.; Chen, M.; Cullen, D. A.; Hwang, S.; Wang, M.; Li, B.; Liu, K.; Karakalos, S.; Lucero, M.; Zhang, H.; Lei, C.; Xu, H.; Sterbinsky, G. E.; Feng, Z.; Su, D.; More, K. L.; Wang, G.; Wang, Z.; Wu, G., Atomically Dispersed Manganese Catalysts for Oxygen Reduction in Proton-Exchange Membrane Fuel Cells. *Nat. Catal.* **2018,** 1, 935-945.

58.   He, Y.; Hwang, S.; Cullen, D. A.; Uddin, M. A.; Langhorst, L.; Li, B.; Karakalos, S.; Kropf, A. J.; Wegener, E. C.; Sokolowski, J.; Chen, M.; Myers, D.; Su, D.; More, K. L.; Wang, G.; Litster, S.; Wu, G., Highly Active Atomically Dispersed CoN_4 Fuel Cell Cathode Catalysts Derived from Surfactant-Assisted MOFs: Carbon-Shell Confinement Strategy. *Energy Environ. Sci.* **2019,** 12, 250-260.

59.   Firouzjaie, H. A.; Mustain, W. E., Catalytic Advantages, Challenges, and Priorities in Alkaline Membrane Fuel Cells. *ACS Catal.* **2020,** 10, 225-234.

60.	Jaouen, F.; Santori, P. G.; Speck, F. D.; Cherevko, S.; Peng, X.; Mustain, W. E.; Varcoe, J. R., Novel Insights in the Activity, Selectivity and Durability of Fenc, Mn-Oxides and Fenc/Mn-Oxide Composites for ORR Catalysis in Alkaline Electrolyte and AEMFC. *Meeting Abstracts* **2019,** MA2019-02, 1671.

61.	Osmieri, L.; Escudero-Cid, R.; Monteverde Videla, A. H. A.; Ocón, P.; Specchia, S., Performance of A Fe-N-C Catalyst for the Oxygen Reduction Reaction in Direct Methanol Fuel Cell: Cathode Formulation Optimization and Short-Term Durability. *Appl. Catal. B Environ.* **2017,** 201, 253-265.

62.	Osmieri, L.; Escudero-Cid, R.; Armandi, M.; Monteverde Videla, A. H. A.; García Fierro, J. L.; Ocón, P.; Specchia, S., Fe-N/C Catalysts for Oxygen Reduction Reaction Supported on Different Carbonaceous Materials. Performance in Acidic and Alkaline Direct Alcohol Fuel Cells. *Appl. Catal. B Environ.* **2017,** 205, 637-653.

63.	Peng, X.; Omasta, T. J.; Magliocca, E.; Wang, L.; Varcoe, J. R.; Mustain, W. E., Nitrogen-Doped Carbon–CoO_x Nanohybrids: A Precious Metal Free Cathode that Exceeds 1.0 W cm^{-2} Peak Power and 100 h Life in Anion-Exchange Membrane Fuel Cells. *Angew. Chem. Int. Ed.* **2019,** 58, 1046-1051.

64.	Varcoe, J. R.; Atanassov, P.; Dekel, D. R.; Herring, A. M.; Hickner, M. A.; Kohl, P. A.; Kucernak, A. R.; Mustain, W. E.; Nijmeijer, K.; Scott, K.; Xu, T.; Zhuang, L., Anion-Exchange Membranes in Electrochemical Energy Systems. *Energy Environ. Sci.* **2014,** 7, 3135-3191.

65.	Pan, Z. F.; An, L.; Zhao, T. S.; Tang, Z. K., Advances and Challenges in Alkaline Anion Exchange Membrane Fuel Cells. *Prog. Energy Combust. Sci.* **2018,** 66, 141-175.

66.	Wang, L.; Peng, X.; Mustain, W. E.; Varcoe, J. R., Radiation-Grafted Anion-Exchange Membranes: the Switch from Low- to High-Density Polyethylene Leads to Remarkably Enhanced Fuel Cell Performance. *Energy Environ. Sci.* **2019,** 12, 1575-1579.

67.   Lei, M.; Wang, Z. B.; Li, J. S.; Tang, H. L.; Liu, W. J.; Wang, Y. G., CeO_2 Nanocubes-Graphene Oxide as Durable and Highly Active Catalyst Support for Proton Exchange Membrane Fuel Cell. *Sci. Rep.* **2014,** 4, 7415.

68.   Lim, C.; Alavijeh, A. S.; Lauritzen, M.; Kolodziej, J.; Knights, S.; Kjeang, E., Fuel Cell Durability Enhancement with Cerium Oxide under Combined Chemical and Mechanical Membrane Degradation. *ECS Electrochem. Lett.* **2015,** 4, F29-F31.

69.   Tobwala, S.; Fan, W.; Hines, C.; Folk, W.; Ercal, N., Antioxidant Potential of Sutherlandia Frutescens and its Protective Effects Against Oxidative Stress in Various Cell Cultures. *BMC complement. Altern. Med.* **2014,** 14, 271.

70.   Zheng, Y.; Omasta, T. J.; Peng, X.; Wang, L.; Varcoe, J. R.; Pivovar, B. S.; Mustain, W. E., Quantifying and Elucidating the Effect of CO_2 On the Thermodynamics, Kinetics and Charge Transport of AEMFCs. *Energy Environ. Sci.* **2019,** 12, 2806-2819.

71.   McCloskey, B. D.; Valery, A.; Luntz, A. C.; Gowda, S. R.; Wallraff, G. M.; Garcia, J. M.; Mori, T.; Krupp, L. E., Combining Accurate O_2 and Li_2O_2 Assays to Separate Discharge and Charge Stability Limitations in Nonaqueous Li–O_2 Batteries. *J. Phys. Chem. Lett.* **2013,** 4, 2989-2993.

Table of Contents Graphic